

Testing the fragmentation limit in the Upper Sco association ^{*}

N. Lodieu^{1,2†}, & N. C. Hambly³, P. D. Dobbie⁴, N. J. G. Cross³, L. Christensen⁵, E. L. Martin⁶, and L. Valdivielso^{7,1,2}

¹ Instituto de Astrofísica de Canarias (IAC), C/ Vía Láctea s/n, E-38200 La Laguna, Tenerife, Spain

² Departamento de Astrofísica, Universidad de La Laguna (ULL), E-38205 La Laguna, Tenerife, Spain

³ Scottish Universities Physics Alliance (SUPA), Institute for Astronomy, School of Physics and Astronomy, University of Edinburgh, Royal Observatory, Blackford Hill, Edinburgh EH9 3HJ, UK

⁴ Australian Astronomical Observatory, PO Box 296, Epping, NSW, 1710, Australia

⁵ Excellence Cluster Universe, Technische Universität München, Boltzmanstrasse 2, 85748 Garching bei München, Germany

⁶ CSIC-INTA Centro de Astrobiología, Ctra. Ajalvir km 4, 28850, Torrejón de Ardoz, Madrid, Spain

⁷ Centro de Estudios de Física del Cosmos de Aragón (CEFCA), Plaza San Juan, 1, E-44001 Teruel, Spain

Accepted 8 September 2021. Received 8 September 2021; in original form 8 September 2021

ABSTRACT

We present the results of a deep ($J \sim 21$ at 5σ) infrared photometric survey of a 0.95 square degree area in the central region of the Upper Sco association. The photometric observations consist of a deep $Y + J$ -band images obtained with the WFCAM camera on the UKIRT InfraRed Telescope (UKIRT) with partly coverage in Z complemented by methane ON and OFF conducted with WIRCAM on the Canada France Hawaii Telescope. We have selected five potential T-type objects belonging to the Upper Sco association on the basis of their blue methane colours and their $J - CH_{4\text{off}}$ colours. We have also identified a sample of 7–8 Upper Sco member candidates bridging the gap between known cluster M-types and our new T-type candidates. These candidates were selected based on their positions in various colour–magnitude diagrams and they follow the sequence of known Upper Sco members identified in the UKIRT Infrared Deep Sky Survey (UKIDSS) Galactic Clusters Survey (GCS). We present additional membership constraints using proper motion estimates from the multiple epochs available to us. We also present optical and near-infrared spectra obtained with the X-Shooter spectrograph on the Very Large Telescope for five L-type candidates covering the 0.6 to 2.5 micron wavelength range, none of them being confirmed as a young brown dwarf. We discuss the lack of detection of new candidate members as well as the possible turn down in the USco mass function as we are approaching the fragmentation limit.

Key words: Stars: low-mass stars and brown dwarfs — techniques: photometric — techniques: spectroscopic — Infrared: Stars — surveys — stars: luminosity function, mass function

1 INTRODUCTION

Knowledge of the shape of the present-day mass function and the masses of the coolest substellar objects in young clusters and star forming regions is of prime importance to put constraints on the formation mechanisms responsible for the existence of brown dwarfs and planetary mass objects.

According to the standard theory of star formation, the fragmentation limit, i.e. the mass at which one object is unable to contract further because it can not radiate its heat to collapse further, is of the order of a few Jupiter masses (5–10 M_{Jup} ; Low & Lynden-Bell 1976; Rees 1976). However, this limit might be lower, possibly of the order of $\sim 1 M_{\text{Jup}}$ in presence of magnetic fields (Boss 2001), but more realistic 3D calculations of the collapse of molecular clouds are required to thoroughly address this issue from the theoretical point of view.

Observationally, several regions have been probed to

^{*} Based on observations collected with the United Kingdom InfraRed Telescope, Canada France Hawaii Telescope, and Very Large Telescope.

† E-mail: nlodieu@iac.es

faint magnitudes at both optical and near-infrared wavelengths to look for a possible cut-off at the low mass end of the mass function. Bihain et al. (2010) reported a possible cut-off below $\sim 6 M_{\text{Jup}}$ in the mass function of the 1–8 Myr-aged σ Orionis cluster from a deep ($J \sim 21.5$ mag) optical/infrared survey over 0.23 square degree. These authors added one further very young objects pre-emptively classified as a T-type candidate to the previously known S Ori 70. The latter object has a T6 spectral type and displays unusual infrared colours pointing towards a younger age (Zapatero Osorio et al. 2002, 2008) but its membership of σ Orionis remains a matter of debate (Burgasser et al. 2004; Scholz & Jayawardhana 2008; Luhman et al. 2008; Peña Ramírez et al. 2011). Alves de Oliveira et al. (2010) presented spectroscopy for a subsample of low mass brown dwarf candidates identified in a survey extending over the full projected area of the ρ Ophiuchus cloud and reaching to $J \sim 20.5$ mag. These authors derive luminosities and effective temperatures for their candidate members but do not present a mass function. Independently, Geers et al. (2011) has confirmed through infrared spectroscopy several candidates as substellar members including one at the deuterium burning limit. Marsh et al. (2010) published the discovery of a T2 dwarf in the same region, finding not confirmed by Alves de Oliveira et al. (2010). Scholz et al. (2009) reported, on the basis of a deep optical and infrared survey of 0.25 square degrees in NGC 1333 complemented by spectroscopy, a possible dearth of planetary mass objects corresponding to a potential cut-off in the cluster mass function in the 20–12 M_{Jup} mass range. Burgess et al. (2009) identified a mid-T-type candidate from a methane survey of ~ 0.11 square degrees in IC 348, suggesting that an extrapolation of the field mass function (Chabrier 2003) may hold in the substellar and planetary mass regimes. Casewell et al. (2007) extracted several L/T-type candidates in 2.5 square degree in the Pleiades cluster from deep optical and infrared photometry complemented by proper motion using the 5 year baseline between both surveys. Evolutionary models (Baraffe et al. 2002) predict masses as low as 10 M_{Jup} for these candidates if indeed members of the Pleiades. The mass function appears to keep rising at such low masses with a slope index which agrees, within the uncertainties, with the values inferred from earlier studies (e.g. Dobbie et al. 2002; Moraux et al. 2003; Lodieu et al. 2007).

The Upper Sco association (hereafter USco) is part of the Scorpius Centaurus OB association: it is located at 145 pc from the Sun (de Bruijne et al. 1997) and its age is estimated to 5 ± 2 Myr from isochrone fitting and dynamical studies (Preibisch & Zinnecker 2002). The association was targeted in X rays (Walter et al. 1994; Kunkel 1999; Preibisch et al. 1998), astrometrically with Hipparcos (de Bruijne et al. 1997; de Zeeuw et al. 1999), and more recently at optical (Preibisch et al. 2001; Preibisch & Zinnecker 2002; Ardila et al. 2000; Martín et al. 2004; Slesnick et al. 2006) and near-infrared (Lodieu et al. 2006, 2007) wavelengths. Several tens of brown dwarfs have now been confirmed spectroscopically as members of the association (Martín et al. 2004; Slesnick et al. 2006; Lodieu et al. 2006; Slesnick et al. 2008; Lodieu et al. 2008; Martín et al. 2010; Lodieu et al. 2011) and the mass function of this population determined well

into the substellar regime (Slesnick et al. 2008; Lodieu et al. 2011).

In this paper we report the outcome of a deep photometric survey of approximately 0.95 square degrees in the central region of USco to (1) find young T-types, (2) test the theory of the fragmentation limit in a young nearby star forming region, and (3) bridge the gap between previous surveys and the new T-type candidates. In Section 2 we describe methane ON and OFF imaging survey obtained with the Canada France Hawaii Telescope (CFHT), the near-infrared *ZYJ* imaging survey carried out with the United Kingdom (UK) InfraRed Telescope (UKIRT), the optical *z*-band imaging obtained with the Wide-Field Camera (WFC) on the Isaac Newton Telescope (INT) and the optical to near-infrared spectroscopy obtained with the X-Shooter instrument on the Very Large Telescope. In Section 3 we outline the photometric selection of T-type candidates using the methane survey complemented by the deep optical *z* band. In Section 4 we attempt to bridge the gap between our previous studies of USco and the search for T-types presented in this paper using various colour-magnitude diagrams drawn from all datasets presented here. We also make use of the multiple epochs to estimate the proper motion of some of the new candidates. In Section 6 we present the X-Shooter spectra of several photometric candidates covering the optical to near-infrared (0.6–2.2 microns) wavelength range. We summarise our investigation in Section 8 and propose future avenues for exploration.

2 IMAGING OBSERVATIONS

In this section, we describe methane ON and OFF, deep *ZYJ*, and optical *z* photometric observations aiming at identifying potential substellar members in USco.

2.1 CFHT WIRCam methane survey

2.1.1 WIRCam Observations

The Wide-field InfraRed Camera (WIRCam; Puget et al. 2004) is a near-infrared (0.9–2.4 microns) camera installed on the prime focus of the 3.6m CFHT on Mauna Kea, Hawaii. WIRCam is equipped with four 2048×2048 HAWAII 2RG detectors. The pixel scale is 0.3 arcsec, thus yielding an almost contiguous field-of-view of 20.5 arcmin aside. We performed observations in February, April, June, and July 2008 with the methane OFF and ON filters which are centered at 1.58 and 1.69 microns, respectively, and covered nine pointings (i.e. one square degree) which are co-incident with our deep *YJ* imaging (the overlapping region is exactly 0.95 square degrees). The centre of the WIRCam coverage is located at $16^{\text{h}} 08^{\text{m}}, -22^{\circ} 45'$, equinox J2000.0. The total time per WIRCam field, including overheads, amounted to 72 min. We used a five point dither pattern with on-source single integrations of 38 sec (see Table 1). The exceptions are for the tiles numbers 5 and 6; our subsequent strategy was optimised to better monitor sky variations at infrared wavelengths. Seeing conditions were generally between 0.6 and 0.8 arcsec at zenith in the *K*-band. Dome flats in the methane OFF and ON filters were taken as part of our program.

Table 1. Log of the CFHT WIRCam photometric observations.

Tile	R.A.	dec	CH _{4on}	CH _{4off}	Date
USco_M1	16:06:40	-23:05	5×14 ^m 24s	5×14 ^m 24	18/02, 19+21/06, 12+15/07/2008
USco_M2	16:06:40	-22:45	5×14 ^m 24s	5×14 ^m 24	24/06, 10+15/07/2008
USco_M3	16:06:40	-22:25	5×14 ^m 24s	5×14 ^m 24	15+16/07/2008
USco_M4	16:08:00	-23:05	5×14 ^m 24s	5×14 ^m 24	16+17/07/2008
USco_M5	16:08:00	-22:45	1×1 ^h 12s	1×1 ^h 12	20+21/02/2008
USco_M6	16:08:00	-22:25	1×1 ^h 12s	5×14 ^m 24	21+25/02, 20+21/04/2008
USco_M7	16:09:20	-23:05	5×14 ^m 24s	5×14 ^m 24	17+18/07/2008
USco_M8	16:09:20	-22:45	5×14 ^m 24s	5×14 ^m 24	11+12/07/2008
USco_M9	16:09:20	-22:25	5×14 ^m 24s	5×14 ^m 24	22+24/04, 18+24+24/06/2008

2.1.2 Data reduction

The data processing of the WIRCam images is done in two steps. First, the detrending (or removal of instrument imprints), done with the “I”iwi pipeline, provides raw and detrended images for our CFHT/WIRCam run. The second stage which involves sky-subtraction, astrometry and photometry is performed with SExtractor (Bertin & Arnouts 1996) at Terapix¹ and outputs fully photometrically and astrometrically calibrated catalogues.

Our observing program produced 729 data cubes, including 702 containing two images and 27 composed of 8 images. The 729 cubes are divided up into 387 and 342 cubes in methane OFF and ON, respectively. However, several images (roughly 100 or 0.06% of the total number of images) had to be removed at different stages of the processing for various reasons, e.g. large extinction due to cloud, the presence of strong electronic noise stripes or other instrument malfunctions.

The detrending steps involve several corrections to remove the cosmetics of the WIRCam infrared detector² and includes flagging of the saturated pixels, non-linearity and reference pixel corrections, dark and flat-field subtraction, bad pixels removal and guiding window masking. The resulting images are then processed by Terapix, following closely the sequence and data flow chart outlined below:

- (i) Creation of masks to identify saturated pixels and reject saturated sources
- (ii) Field to field relative astrometric and photometric calibration. The initial global astrometric calibration is based on the 2MASS point source catalogue (Cutri et al. 2003; Skrutskie et al. 2006)
- (iii) Generate a first stack with the detrended and sky-subtracted images for each filter to estimate the sky background after removal of the faintest sources. The stacked images represent the weighted median of the individual images combined with the Lanczos3 interpolation kernel. The reference coordinate system is the FK5 or J2000 system with the distorted tangential projection type
- (iv) Sky subtraction is made in two steps and created from a sample of 30 images before subtracting the sky from the detrended images

(v) In some cases sky masking has to be implemented in addition to the normal procedure if it turned out to be impossible to estimate the sky level for some pixels

(vi) Assessment of the quality of sky-subtracted images and catalogues. After visual inspections, a few images (< 20) had to be rejected due to luminosity gradients, cosmetics defects or large scale patterns

The final step consists of generating sky-subtracted images to compute the astrometric and relative photometric calibration with field to field rescaling. Individual stacks were created for the 18 images in methane OFF and ON as well as two mosaics containing the nine pointings of each filter. The catalogues, generated with SExtractor (Bertin & Arnouts 1996), contain the pixel and world coordinates, aperture fluxes and magnitudes with their associated errors as well as quality flags. The final merged catalogue with the methane ON and OFF data contains 166,265 sources, of these 131,937 have quality flags equal to zero indicating that they are robust detections. There are 92,918 sources with photometric error bars less than 0.3 mag in the methane colour. The completeness limit of the methane survey is 20.3 and 20.2 mag in the CH_{4off} and CH_{4on}, respectively. These limits are deduced from the points where the histograms deviate from a powerlaw fit to the counts.

2.2 Deep UKIRT WFCAM ZYJ survey

2.2.1 WFCAM Observations

The UKIRT wide-field camera (WFCAM) is equipped with four 2048×2048 Rockwell detectors spaced by 94% and sensitive to near-infrared (1.0–2.5 microns) wavelengths (Casali et al. 2007). The pixel size is 0.4 arcsec, giving a coverage of 0.19 square degree in a single exposure (called pawprint). Four pawprints are required to fill in the gaps between the detectors and cover a filled square of 0.75 square degree (or tile). The camera is equipped with several filters, including the Z and Y filters specific to WFCAM as well as the standard Mauna Kea Observatory (Tokunaga et al. 2002) JHK filters (Hewett et al. 2006).

We have conducted a deep Y, J imaging survey with WFCAM of the central region in the USco previously surveyed by the UKIRT Infrared Deep Sky Survey (UKIDSS) Galactic Clusters Survey (GCS) (Lodieu et al. 2007). The observations took place in May and June 2008 (Table 2). Weather conditions were generally good with clear skies and

¹ <http://terapix.iap.fr/>

² More details on the pre-processing of WIRCam images at www.cfht.hawaii.edu/Instruments/Imaging/WIRCam/liwiVersion1Doc.html

Table 2. Log of the UKIRT WFCAM photometric observations.

Tile	R.A.	dec	Repeat	Date	Seeing
#1	16:06:00	-23:09:00	4× <i>J</i>	03May2008	1.0''
#1			1× <i>J</i>	04May2008	~0.9''
#1			4× <i>Y</i>	04May2008	~0.9''
#1			1× <i>Z</i>	03Jun2008	~1.0''
#2	16:13:12	-22:15:00	5× <i>J</i>	05May2008	0.5–1.0''
#2			2× <i>Y</i>	30May2008	~1.0''
#2			2× <i>Y</i>	31May2008	~0.7''

seeing better than 1.0 arcsec as measured on the images. We have obtained eight pawprints in the *Y* and *J* filter, covering a total of ~1.7 square degrees. An additional *Z*-band image was obtained for four pawprints because of the high airmass of USco from Mauna Kea and our seeing requirements which hampered achieving regularly seeing better than 1.2 arcsec in this filter. The central coordinates of each pawprint are provided in Table 2. The on-source individual exposure times were set to 22.25, 20, and 10 seconds in the *Z*, *Y*, and *J* filters, respectively, repeated twice in *Z*, *Y* and three times in *J*. We used a 2×2 microstepping pattern and a 5 point dither arrangement with offsets of 3.2 arcsec to subtract the sky properly. We reached depths of 5 σ at 22.0–22.3 mag and 21.5–21.7 mag in *Y* and *J*, respectively. The resulting (*Y* – *J*, *Y*) colour-magnitude diagram is displayed in Figure 1. We observe a gap between potential members and field stars as previously reported in our studies of USco (Lodieu et al. 2006, 2007) and the Pleiades (Lodieu et al. 2007). However, as we discuss in the next sections, most of the new photometric candidates identified in this deep survey which follow the sequence of USco spectroscopic members turn out to be non-members.

2.2.2 Data reduction

All data taken with WFCAM were reduced automatically by the Cambridge Astronomy Survey Unit (CASU)³ even if there are not part of the UKIDSS project (Lawrence et al. 2007). The description of the automatic pipeline data reduction is explained in Irwin et al. (2004) with additional updates detailed on the CASU webpage⁴. The processing involve several technical steps before generating the final photometric catalogues, including flat fielding, sky subtraction, correction for field distortion, removal of low level pseudo-periodic ripples in dark images (or decurtaining), and removal of persistence and crosstalk artifacts due to the presence and reminiscence of bright stars on infrared detectors. The catalogues can then be retrieved from the WFCAM Science Archive (WSA; Hambly et al. 2008) to extract the astrometry and photometry.

As a consequence of multiple repeats of each pawprint for each filter, an additional step was necessary to combine all images of each pawprint in each filter. At WFAU

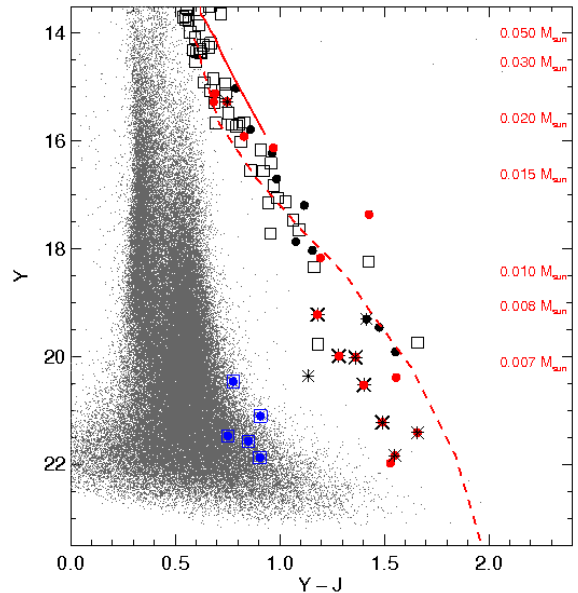


Figure 1. (*Y* – *J*, *Y*) colour-magnitude diagram for ~1.7 square degree in USco. The small dots are all sources detected along the line of sight of the association. Open squares are spectroscopically confirmed members of the USco association from the UKIDSS GCS (Lodieu et al. 2007, 2008). Black filled circles are photometric candidates identified in the deep *YJ* survey alone, the red circles being new ones. Asterisks are later classified as photometric and/or spectroscopic non members using additional datasets presented in this paper. Blue circles with blue open squares are the five methane candidates undetected in the optical and with *Y*, *J* photometry. Overplotted are the NextGen (solid line; Baraffe et al. 1998) and DUSTY (dashed line; Chabrier et al. 2000) 5 Myr isochrones shifted at a distance of 145 pc.

(Wide Field Astronomy Unit) pawprints from each minimum scheduled block (MSB) were first subjected to quality control using an automated set of procedures, and those that were deemed acceptable were used in all further curation and released and the others were deprecated (see Collins et al. 2009, for details). The quality controlled pawprints were then grouped together, using the metadata in the WSA tables. The grouping occurred in two stages: first by position to find all unique pointings (where pointings were within 4 arcmin of each other) and then grouped by pointing, filter and level of microstepping to determine deep products. If a particular pointing and filter combination contains more than one level of microstepping, then the level of microstepping that corresponds to data with the greatest total exposure time is selected on a product-by-product basis. The stacking code used can only deal with one level of microstepping, so this is a necessity.

Deep pawprint stacks and confidence images were then created by looping through the list of stacks and selecting pawprint science frames (the stacks created from processing each MSB) that match the pointing, filter and microstep criteria. The CASU code “fitsio_stack” was used for the stacking, and then a catalogue was created for each stack using the codes “cir_imcore”, “cir_classify” and “cir_catcoord”, all produced at CASU (see Irwin et al. in prep). The new deep stacks and catalogue data were then ingested into the WSA.

³ <http://casu.ast.cam.ac.uk>

⁴ <http://casu.ast.cam.ac.uk/surveys-projects/wfcam/technical>

The merged passband source table was produced from the deepest data in each pointing/filter, i.e. from the deep stack catalogues. Hambly et al. (2008) provides details on the production and contents of the Source table. Multi-epoch tables were produced as described in Cross et al. (2009). The final combined catalogues could then be retrieved directly with a Structured Query Language (SQL) query sent through the WSA webpage.

2.3 INT WFC optical z -band imaging

2.3.1 INT Observations

The Issac Newton Telescope (INT) is a 2.54-m optical telescope currently equipped with two instruments, one of which being a wide-field camera (WFC) located at its prime focus. The WFC consists of four thinned EEV 2048×4096 Charge-Coupled Devices (CCDs), offering a field-of-view of approximately 34 arcmin and a pixel size of 0.33 arcsec. The inter-spacing between the CCDs is small, resulting in a loss of coverage of the order of 1 arcmin.

We carried out a z -band imaging survey of the full coverage of the GCS Science Verification phase presented in Lodieu et al. (2007) over several nights on 19–25 April 2006. In this paper, we mainly focus on the area overlapping with the methane and deep YJ survey to complement the near-infrared photometry and add constraint on the membership of potential cluster member candidates. The nights of 19 and 25 April offered excellent weather with good seeing and stable conditions. The weather conditions on 20 April were also good but the seeing was variable. The night of 21 April was completely lost due to high humidity. The nights on 22 and 23 April were windy and the night on 24 April had humidity of 80%.

2.3.2 Data reduction

The WFC data were reduced using the Cambridge Astronomical Survey Unit CCD reduction toolkit (Irwin & Lewis 2001) to follow standard steps, namely, subtraction of the bias, non-linearity corrections, flat-fielding and astrometric calibration. However, in addition, each frame was corrected for fringing using a fringe map constructed from a clipped stack of the images from all our pointings. Subsequently, photometry was performed on the reduced images using a circular window with a diameter of $1.5\times$ the full width half maximum of the mean point spread function. Finally, we created catalogues of all the sources detected in the frames and morphologically classified these as either stellar or non-stellar. We haven't calibrated photometrically the INT images with a specific standard star but instead used the WFCAM Z -band from the Science Verification phase to estimate the depth of the INT observations. We estimate the 3σ depths to $Z=20.7\text{--}21.1$ mag on the 19, 23–25 April 2008 while images taken on 20 and 22 April are shallower with depths of 20.0 ± 0.2 and 19.5 ± 0.3 , respectively. Thus, the INT images are usually deeper than the UKIDSS GCS survey, except for the observations on 20 and 22 April 2008. Note that these depths are given in the WFCAM Z filter and not the INT z filter.

2.4 Spectroscopic observations

2.4.1 X-shooter observations

We carried out optical to near-infrared spectroscopy with the UV- to K -band intermediate resolution ($R\sim 3500$), high efficiency spectrograph X-shooter (D'Odorico et al. 2006) mounted on the Cassegrain focus of the Very Large Telescope (VLT) Unit 2. Observations were carried out over several nights during period 85 (April to September 2010) in service mode by the staff at Paranal, Chile. The log of the observations is detailed in Table 3. Weather conditions met our initial requirements: no constraints on the moon, seeing better than 1 arcsec (satisfied in most cases), and thin cirrus acceptable.

X Shooter is a multi wavelength cross-dispersed echelle spectrograph made of three independent arms covering simultaneously the ultraviolet (UVB; 0.3–0.56 microns), visible (VIS; 0.56–1.02 microns), and near-infrared (NIR; 1.02–2.48 microns) wavelength ranges thanks to the presence of two dichroics splitting the light. The spectrograph is equipped with three detectors: a 4096×2048 E2V CCD44-82, a 4096×2048 MIT/LL CCID 20, and a 2096×2096 Hawaii 2RG for the UVB, VIS, and NIR arms, respectively. We used the 1.5 arcsec slit (1.6 arcsec for the UVB arm) to achieve a nominal resolution of 3300 (9.9 pixel per full-width-half-maximum) in the UVB and NIR arms and 5400 (6.6 pixel per full-width-half-maximum) in the VIS arm.

All observations were carried out at parallactic angles. The X-Shooter acquisition is made through an optical CCD, implying that our targets are not visible on the images obtained by the acquisition camera screen. Therefore, we used nearby reference stars to put our targets on the slit. Unfortunately, due to an error in the offset computation, one candidate, USco J160812.99–230431.43, observed in April 2010 was out of the slit and we do not have spectra for it. The exposure times were scaled according to the brightness of the target (see Table 3) to achieve a minimum signal-to-noise of 20 after degrading the resolution by a factor of 5. Calibrations were taken according to the instrument calibration plan, including bias, dark, flat field and arc frames. The spectra of four confirmed photometric candidates, normalised at 1.265 microns, are displayed in Figure 4.

2.4.2 Data reduction

We reduced the X-Shooter spectra on each arm independently using version 1.3 of the pipeline and following the instructions described in the manual ((Issue 4; 30 november 2010) Goldoni et al. 2006; Modigliani et al. 2010). None of the five targets have flux in the ultraviolet arm (UVB) so we do not discuss these data further.

We followed the steps enumerated in the manual using the physical model option to construct a final 2D spectrum for each target and its respective standard star both in the visible (VIS) and infrared (NIR) arm. First, we created a bad pixel map for the NIR detector using a set of 40 linearity frames aimed at identifying non-linear pixels. This step is not required for the VIS arm. Next, we created a master bias and master dark for the VIS and NIR arm, respectively. Afterwards, we determined a first guess order and then we refined the line tables by illuminating the X-Shooter pinhole with a continuum lamp. Later, we created a master flat and

Table 3. Log of the X-Shooter spectroscopic observations. Note that USco J160835.54–225311.4 was observed three times. Note that USco J160812.99–230431.43, not listed in this table, was out of the slit due to an error in the offset computation.

ID	R.A.	dec	<i>J</i>	Date	ExpT	Seeing	Airmass	Reference star
4	16:07:55.42	–22:33:52.52	18.039	24Apr2010	20min	0.60–0.69	1.010	16:07:56.07 –22:33:24.6 (<i>I</i> =10.60 mag)
7	16:08:42.38	–22:23:25.86	18.649	29Jul2010	45min	0.64–0.67	1.087	16:08:43.92 –22:23:29.4 (<i>I</i> =14.47 mag)
3	16:07:16.98	–22:42:14.06	19.730	11Jun2010	60min	0.66–0.68	1.212	16:07:14.41 –22:41:59.8 (<i>I</i> =15.45 mag)
8	16:09:00.40	–23:11:50.95	19.751	26Jul2010	60min	1.14–1.26	1.122	16:09:02.01 –23:12:04.11 (<i>I</i> =14.06 mag)
6	16:08:35.54	–22:53:11.37	20.284	19Aug2010	40min	1.25–1.30	1.038	16:08:38.72 –22:53:04.0 (<i>I</i> =15.09 mag)
6	16:08:35.54	–22:53:11.37	20.284	19Aug2010	40min	1.25–1.30	1.111	16:08:38.72 –22:53:04.0 (<i>I</i> =15.09 mag)
6	16:08:35.54	–22:53:11.37	20.284	20Aug2010	40min	0.85–0.96	1.056	16:08:38.72 –22:53:04.0 (<i>I</i> =15.09 mag)

an order table tracing the flat edges before establishing the two-dimensional map of the instrument. Subsequently, we determined the efficiency of the whole system made of the telescope, instrument, and detector. Finally, we generated a 2D spectrum in stare mode for the target and its associated standard, both in the VIS and NIR arms.

The next steps were carried out under the IRAF environment⁵ although an optimal extraction option is available in the pipeline’s release. First, we extracted a 1D spectrum from the 2D images of the VIS and NIR arm for the target and the star star using the IRAF routine `APSUM`. Only few spectrophotometric standard stars have been fully calibrated from the UV to the near-infrared spectral range at the time of writing. For this reason, all of our targets are associated with the GD 153 white dwarf standard, except candidate number 6 which was observed just before another white dwarf standard, Feige 110. We downloaded the calibrated spectra of GD 153 and Feige 110 originating from observations conducted with the Hubble Space Telescope and covering the UVB, VIS, and NIR arms⁶. Afterwards, we divided the 1D spectrum of the standard star from the 1D spectrum of the science target and multiplied by the Hubble spectrum of GD 153 and Feige 110 for candidates 1 to 5 and candidate, respectively.

The X-Shooter spectra are contaminated by the presence of sky lines. We attribute this to the current version (Issue 1.3) of the pipeline which is not yet optimised to minimise the residuals of the numerous sky lines present over the full wavelength range covered by X-Shooter, particularly in the stare mode reduction. The near-infrared (1.0–2.25 microns) spectra of four photometric candidates resembling L-types are displayed in Figure 4. The optical spectra of USco J160842.38–222325.86 and USco J160716.98–2242.1406 are shown in Figure 5; the other two objects exhibiting no flux blueward of 1 μ m. The spectrum of USco J160900.40–231150.95 classifies it as a quasar at a redshift of 0.8789 and is discussed in more detail in Section 6.2.

3 SEARCH FOR CLUSTER T-TYPE CANDIDATES

A search for T-type candidate members of the USco Association is likely easier than for the Trapezium Cluster and the Pleiades due to a combination of it’s age and distance. Indeed, the apparent magnitude of a 3 M_{Jup} T-type (effective temperature below ~ 1100 K) at 5 Myr and 145 pc is predicted to be ~ 0.5 and ~ 4.5 mag brighter in *J* than in the Trapezium Cluster and the Pleiades, respectively, based on the COND models for dust-free brown dwarfs (Baraffe et al. 2002). Furthermore, USco exhibit a significant proper motion ($-11, -25$ mas/yr de Zeeuw et al. 1999) so that the membership of any T-type candidate could be confirmed (or otherwise) with a 3 to 5 year baseline. Finally, star formation has ended in USco (Walter et al. 1994) and the region we have focused our deep survey on has low foreground extinction ($A_V \leq 2$ mag; Preibisch et al. 1998).

In this section, we describe our photometric selection of cluster T-types starting from the methane imaging alone. Then, we look at their optical photometry using the INT data. Afterwards, we investigate their *Y, J* photometry to check if these are consistent with T-type members of USco.

The absolute *J* magnitudes of old (>1 Gyr) field T-type brown dwarfs are fainter than $M_J \sim 13.5$ –14.0 mag (Vrba et al. 2004; Liu et al. 2007; Leggett et al. 2010; Marocco et al. 2010), corresponding to an apparent magnitude of $J \sim 19.3$ –19.8 mag at the distance of USco. The *H*-band absolute magnitude is roughly 0.5 mag brighter. Therefore, we proceed as follows to select potential “methane” candidates. We considered only sources with error bars on their methane colour less than 0.3 mag. First, we computed the median values of the methane colour, per 0.5 mag interval of the methane OFF band from 17.5 to 21 mag (Table 4). We set the brightness limit to 17.5 mag to account for the fact that substellar objects are brighter when younger, and the blue *J – H* and *H – CH_{4off}* trends exhibited towards lower temperatures – for example, there is a difference of about one magnitude for a 5 Myr-old 1000 K brown dwarf compared to a 1 Gyr T-type brown dwarf at the same effective temperature (Burrows et al. 1997; Chabrier & Baraffe 1997). Then, we calculated the median absolute deviation (MAD) i.e. the median of the set of absolute values of deviation from the central value computed as above. Finally, we selected as potential candidates all those objects lying 3σ to the blue of the median methane value in each bin where σ was robustly computed as $1.48 \times \text{MAD}$. The median and

⁵ IRAF is distributed by National Optical Astronomy Observatory, which is operated by the Association of Universities for Research in Astronomy, Inc., under contract with the National Science Foundation.

⁶ Ascii files containing fluxes from the ultraviolet to the near-infrared can be downloaded from <http://www.stsci.edu/hst/observatory/cdbs/calspec.html>

Table 4. Statistical selection of potential candidates in USco from the methane survey. ‘Median’ is the median value of the methane colour in each magnitude interval; STD is the standard deviation, ‘Nb’ is the number of objects used to compute the median and standard deviation, and the last column represents the number of candidates satisfying the 3σ methane selection.

J range	Median	σ	Nb	Candidates
17.5–18	-0.060	0.058	3478	863
18–18.5	-0.079	0.080	4497	1088
18.5–19	-0.109	0.114	6027	1398
19–19.5	-0.148	0.155	8226	1846
19.5–20	-0.209	0.217	9943	1934
20–20.5	-0.288	0.290	10452	870
20.5–21	0.338	0.339	7121	19
17.5–21	—	—	49744	8018

σ values are reported in Table 4 along with the number of candidates.

To eliminate contaminants, we cross correlated this large list of candidates with the INT optical photometric catalogue using a matching radius of 2 arcsec. We found 5410 sources with optical photometry out of the 8018 methane candidates, implying that 2608 have no detected optical counterpart. About 65% of those candidates without optical counterpart down to the depth of the INT survey are covered by the deep YJ data, leaving about 1750 sources to investigate further. Among these ~ 1750 sources, 806 have a counterpart within 2 arcsec in the deep YJ survey.

We investigated the near-infrared photometry of these 806 candidates to reject contaminants. We computed the $J - CH_{4\text{off}}$ colours for each candidate and considered only sources bluer than 0.5 mag in $J - CH_{4\text{off}}$ (Tinney et al. 2005; Goldman et al. 2010; Peña Ramírez et al. 2011). Applying this colour cut leaves one object with a negative $J - CH_{4\text{off}}$ colour, one object with $J - CH_{4\text{off}} \leq 0.2$ mag, 4 candidates with $J - CH_{4\text{off}} = 0.25\text{--}0.30$ mag, 12 candidates with $J - CH_{4\text{off}} = 0.3\text{--}0.4$ mag, and 26 candidates with $J - CH_{4\text{off}} = 0.4\text{--}0.5$ mag. However, we discarded the candidate with the bluest $Y - J$ colour because it turned out to be a mismatch. Additionally, we rejected 13 of these sources as they were detected in the WFCAM Z imaging and a further 29 with $Y - J$ colours that are too blue ($Y - J \leq 0.7$ mag; including 4 already detected on the WFCAM Z images) to be consistent with T-type members. Thus there are 5 candidates which remain of interest to us. We checked those five sources in the WFCAM YJ (no Z -band images available) and the WIRCam methane images to detect any false positive but did not find any. The bluest object in $J - CH_{4\text{off}}$ and thus the most interesting candidate, has a methane colour of -0.87 mag and $Y - J = 0.85 \pm 0.10$. The coordinates and photometry of these candidates is provided in Table 5.

We looked at the images of the recent data release of the Wide-Field Infrared Survey Explorer (WISE; Wright et al. 2010) to check whether these T-type candidates are detected at 3.4 and 4.6 microns. None of the five candidates are detected. However, non-detections do not constitute a strong constraint on their spectral type since T-types exhibit $J - 3.4$ and $J - 4.6$ colours in the 2–4.5 and 0–3 mag range (Patten et al. 2006; Leggett et al. 2010; Mainzer et al.

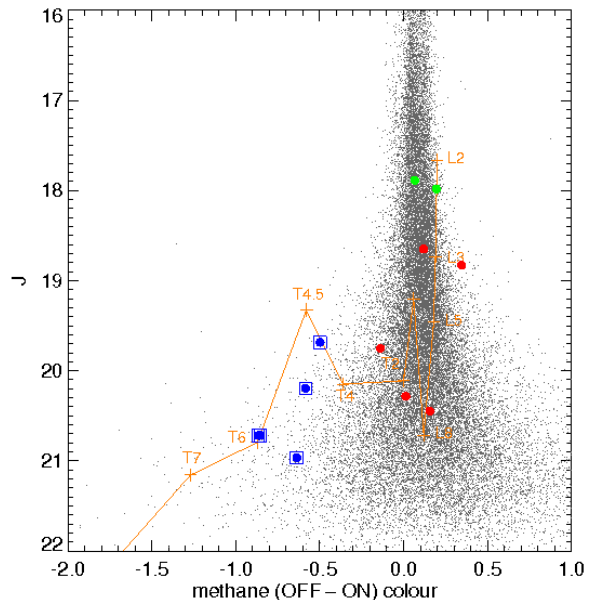


Figure 2. ($CH_{4\text{off}} - CH_{4\text{on}}, J$) colour-magnitude diagram for ~ 0.95 square degree in USco. The small grey dots are all sources detected in the deep YJ survey with methane photometry. Green symbols are USco photometric candidates with a near-infrared spectrum: the bluer object is a field L2 dwarf whereas the redder source is L1 dwarf member of USco. Red dots are new candidates selected from the deep YJ survey for which methane photometry is available. Overplotted are synthetic colours for spectral types L2, L3, L5, L8, T0, T2, T4, T4.5, T6, T7, and T8 (orange lines with plus signs to mark the spectral types; Tinney et al. 2005). Blue circles surrounded by open squares are the five methane candidates undetected on the INT images and with Y, J counterparts.

Table 5. Photometry for the methane T-type candidates without optical counterparts and detected in the deep YJ survey. The last column gives a priority (P) of interest, 1 being the highest.

R.A.	dec	Y_{deep}	J_{deep}	$CH_{4\text{off}}$	$CH_{4\text{on}}$	P
16:08:35.98	-22:29:11.1	21.869	20.964	20.471	21.108	3
16:08:45.73	-22:29:53.5	21.469	20.718	20.290	21.145	3
16:08:47.80	-22:29:04.5	21.568	20.718	20.585	21.450	1
16:09:55.91	-22:33:45.7	21.103	20.194	19.811	20.395	2
16:10:04.76	-22:32:30.6	20.462	19.685	19.257	19.754	3

2011) which does not guarantee a mid-infrared detection at to the WISE sensitivities (16.5 and 15.5 mag at 3.4 and 4.6 microns, respectively).

4 BRIDGING THE GAP BETWEEN M AND T-TYPES

In this section we describe the photometric selection employed to identify further USco member candidates in the area common to the deep YJ survey and methane imaging. Additional membership constraints are derived from the infrared Z photometry as well as crossmatching with

the UKIDSS GCS (Lodieu et al. 2007) and its associated spectroscopic follow-up (Lodieu et al. 2008, 2011).

We found that the USco sequence is well separated from field stars in several colour-magnitude diagrams (including the $(Y - J, Y)$ diagram) from the central region surveyed during the Science Verification (SV) phase of the UKIDSS GCS (Lodieu et al. 2007). The cluster sequence extends down to $10 M_{\text{Jup}}$ and possibly below depending on the validity of the mass estimates provided by current theoretical models (Baraffe et al. 2002). We note that we clearly detect the M7/M8 gap at $Z \sim 15.5$ mag and $J \sim 14$ mag proposed to by Dobbie et al. (2002).

We started off our photometric selection using the $(Y - J, Y)$ colour-magnitude diagram (Figure 1). We used the sample of spectroscopic members extracted from the UKIDSS GCS (Lodieu et al. 2008) to define our selection criteria. The sequence appearing in the deep $(Y - J, Y)$ colour-magnitude diagram matches well the sequence previously seen in the GCS SV data (Lodieu et al. 2007) after applying the offset of +0.08 mag to the SV data (see “Known Issues” for UKIDSS Data Release 3 in the WSA). We queried the WSA to extract coordinates and photometry of all point sources with good quality fainter than $J = 10.5$ mag (saturation level of the deep survey). This catalogue contains 172,209 objects. However, we focused our search only on sources fainter than $Y = 15$ mag because we aim to uncover USco members with masses below $\sim 30 M_{\text{Jup}}$ and, more specifically, 5 Myr-old L- and T-types. Similarly, we considered only sources brighter than the 5σ detection limit in Y i.e. $Y \leq 22.2$ mag. As a consequence, we picked out all objects to the right of a line extending from $(Y - J, Y) = (0.65, 15.0)$ to $(1.50, 22.0)$ in the $(Y - J, Y)$ diagram. This selection returned 30 sources detected in Y and J , including three with Z -band photometry. Among these 30 sources, four have been removed from the final candidate list because they were either residual crosstalk artifacts (three objects) or at the edge of the detector (one object). Thus, we are left with 26 reliable candidates which warrant further investigation.

We crossmatched these 26 candidates against the list of members identified in the GCS SV, resulting in ten common sources (Table 6). We have recovered all candidates from our GCS SV work in our selection. Eight of them are known spectroscopic members with spectral types ranging from M8 to L1 (Lodieu et al. 2008), one is classified as a spectroscopic non member (USco J160956.34–222245.5; dL2; Lodieu et al. 2008), and the remaining one has an optical spectral type (USco J161154.39–223649.3; M6.25) from our multi-fibre spectroscopic follow-up (Lodieu et al. 2011). We note that the new $Y - J$ colour (1.55 ± 0.06 mag) of USco J160843.43–224516.1 differs from the old measurement from the GCS SV ($Y - J = 1.18 \pm 0.20$), putting this object back on the cluster sequence in the $(Y - J, Y)$ diagram. We conclude that this spectroscopic member may be variable and/or may possess circumstellar material.

To further constrain the membership of the 16 new candidates, we looked for additional photometry in Z , H , and K in the deep Z -band survey, in the latest release of the UKIDSS GCS (Data Release 8 in September 2010) and in the GCS SV database. Two objects are detected in the deep Z image and show magnitudes consistent with the photometry extracted from the SV database within the

Table 6. Coordinates (in J2000), near-infrared YJ magnitudes and their associated photometric error bars for the 10 candidates extracted from our deep YJ survey and already identified in the GCS Science Verification survey (Lodieu et al. 2007). The last column provides the spectral types derived from spectroscopy (Lodieu et al. 2008, 2011).

R.A.	dec	$Y \pm \text{err}Y$	$J \pm \text{err}J$	SpT
16:06:48.18	−22:30:40.2	15.787±0.003	14.928±0.002	M8/M8.5
16:07:27.83	−22:39:04.0	18.030±0.008	16.873±0.006	L1
16:07:37.98	−22:42:47.0	17.865±0.008	16.788±0.006	L0
16:08:18.43	−22:32:25.1	17.194±0.005	16.077±0.004	L0
16:08:43.43	−22:45:16.1	19.912±0.030	18.358±0.015	L1
16:08:47.45	−22:35:47.9	16.701±0.004	15.716±0.004	M9
16:09:18.68	−22:29:23.8	19.457±0.020	17.981±0.012	L1
16:09:56.34	−22:22:45.6	19.302±0.019	17.887±0.011	dL2 (NM)
16:10:47.14	−22:39:49.5	16.218±0.003	15.254±0.003	M9/M8.5
16:11:54.39	−22:36:49.3	15.015±0.002	14.225±0.002	M6.25

error bars (Table 7). Their positions in the $(Z - J, Z)$ diagram (Top, left panel in Figure 3; see also Figure 3 of Lodieu et al. 2007) place them at the border between the field stars and the cluster sequence. Additionally, we extracted H and K photometry from GCS DR8 for 13 out of 16 new candidates. The other three sources lie in a gap within the GCS SV coverage due to control quality rejection in the SV data (see Figure 1 in Lodieu et al. 2007). We plotted these 13 sources in the $(Y - K, Y)$ and $(J - K, J)$ colour-magnitude as well as in the $(H - K, J - H)$ colour-colour diagram (Figure 3) along with spectroscopically confirmed USco members to assess their membership. Four candidates (USco J160755.42–223352.5; USco J161257.41–230555.4; USco J160842.38–222325.9; USco J161105.28–222257.3) are classified as photometric non members because they exhibit blue colours in several diagrams (asterisks in Figure 3). There is another object (USco J160716.98–224214.1) for which only K -band data is available, suggesting that it is also a photometric non member due to its blue infrared colours (asterisk in Figure 3). The remaining eight candidates remain bona-fide members of the USco association. Finally, we have added a photometric constraint using the Z photometry from the GCS SV for seven sources out of the 16. The brightest candidates are confirmed as photometric candidates (top left panel of Figure 3) while the two faintest sources (USco J161105.28–222257.3 and USco J160755.42–223352.5) are rejected due to their blue $Z - J$ colours (note that they were already rejected based on their $Y - K$ and $J - K$ colours).

Some of the 16 new candidates are quite bright but were not selected as potential members in the SV survey. Seven of them are, however, in the SV coverage with $YJHK$ photometry and should have been recovered if indeed members (Table 7). The two faintest, USco J160755.42–223352.5 and USco J160842.38–222325.9, are photometric non members due to their blue infrared colours as discussed above. The remaining five are much brighter. One object, USco J161000.17–231219.3, was included in our AAOmega optical follow-up and classified as a spectroscopic non member on the basis of its strong NaI doublet (Table C.1 in Lodieu et al. 2011). USco J160903.86–222322.2

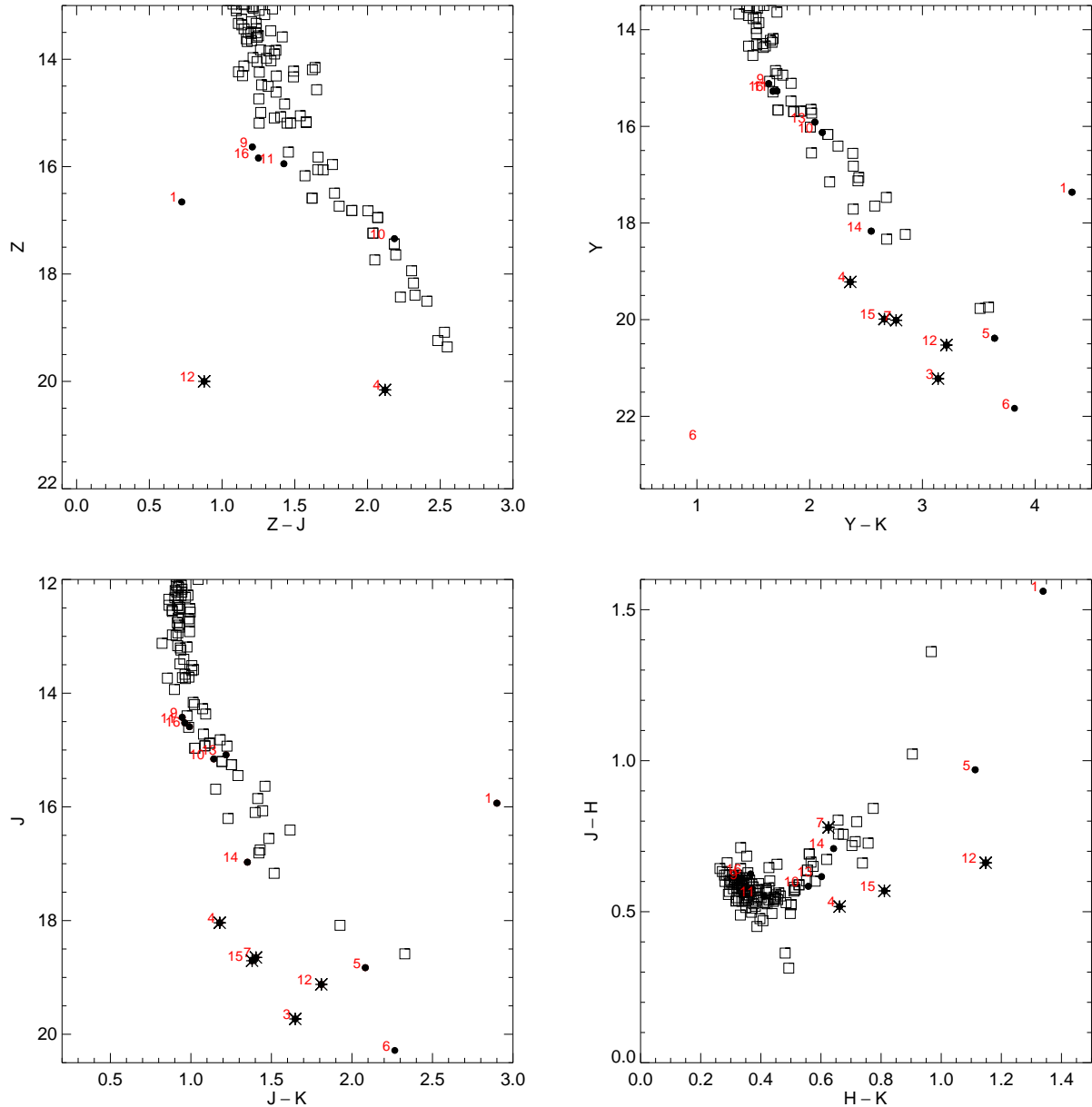


Figure 3. *Top left:* $(Z - J, Z)$ colour-magnitude diagram. *Top right:* $(Y - J, Y)$ diagram. *Bottom left:* $(J - K, J)$ diagram. *Bottom right:* $(H - K, J - H)$ colour-colour diagram. The diagrams show the location of the new candidates identified in our deep YJ survey (filled circles) along with previously known spectroscopic members of USco from the UKIDSS GCS (open squares). Photometric non members are marked with black asterisks. The numbers correspond to the candidates listed in Table 7 in the same order (i.e. ordered by right ascension).

and USco J161330.35–224406.7 are clear proper motion non members based on our estimate from the 2MASS/GCS SV crossmatch, a hypothesis corroborated by the US Naval Observatory measurements (Monet et al. 2003). USco J160905.67–224517.0 was also classified as a proper motion non member from our 2007 study but lies very close to the 2σ proper motion selection. Finally, USco J160630.92–225815.2 appears as a bona-fide photometric and proper motion member from our SV study and the new deep survey. The Y and J magnitudes became fainter by approximately 1.4 and 1.0 mag, respectively, between the SV and deep survey epochs.

This source was also included in our AAOmega multi-fibre spectroscopic follow-up (Lodieu et al. 2011) and its spectrum suggests that it is a young active star with strong $H\alpha$, Helium, NII, and SII emission lines and whose continuum is rising steeply from 6000 to 9000 Å. Overall we have rejected sources which do not satisfy at least two colours criteria or a colour and proper motion or spectroscopic criteria. The final membership is given in the last column of Table 8 and a note has been added to Table 7 for the three sources not in Table 8. The other bright candidates identified in this paper could not have been recovered by our SV study because we

Table 7. Coordinates (in J2000), near-infrared *ZYJ* magnitudes from the deep survey, *Z* photometry from the Science Verification phase (not yet available in GCS DR8), *H* and *K* from the latest UKIDSS GCS data release, and methane ON and OFF magnitudes with their associated photometric error bars for the 16 new candidates. The sources are ordered by right ascension and the first column provide an identifier reported in the figures and other tables.

^a This object remains as photometric candidate

^b This object is a field L dwarf spectroscopically

^c Classified as quasar spectroscopically.

ID	R.A.	dec	Z_{deep}	Y_{deep}	J_{deep}	H_{DR8}	K_{DR8}	Z_{SV}	$\text{CH}_{4\text{off}}$	$\text{CH}_{4\text{on}}$
1	16:06:30.92	-22:58:15.2	—	17.362±0.006	15.935±0.004	14.374±0.005	13.035±0.003	16.658±0.011	—	—
2	16:06:46.45	-22:31:23.8 ^a	—	21.977±0.187	20.448±0.081	—	—	—	19.562±0.094	19.405±0.071
3	16:07:16.98	-22:42:14.1 ^b	—	21.221±0.095	19.730±0.045	—	18.082±0.208	—	—	—
4	16:07:55.42	-22:33:52.5	20.357±0.027	19.220±0.018	18.039±0.013	17.522±0.070	16.860±0.065	20.159±0.178	—	—
5	16:08:12.99	-23:04:31.4	—	20.385±0.053	18.828±0.022	17.858±0.102	16.745±0.065	—	17.847±0.020	17.501±0.013
6	16:08:35.54	-22:53:11.4	—	21.835±0.171	20.284±0.069	18.220±0.144	18.018±0.196	—	19.760±0.092	19.747±0.061
7	16:08:42.38	-22:23:25.9	—	20.012±0.030	18.649±0.018	17.870±0.094	17.245±0.091	—	17.804±0.019	17.685±0.008
8	16:09:00.40	-23:11:51.0 ^c	—	21.410±0.112	19.751±0.044	—	—	—	19.962±0.279	20.100±0.204
9	16:09:03.86	-22:23:22.2	15.693±0.003	15.116±0.002	14.425±0.002	13.817±0.003	13.479±0.003	15.633±0.006	—	—
10	16:09:05.67	-22:45:16.7	—	16.126±0.003	15.156±0.003	14.572±0.006	14.014±0.005	17.341±0.019	—	—
11	16:10:00.17	-23:12:19.3	—	15.270±0.002	14.522±0.002	13.971±0.004	13.560±0.004	15.947±0.007	—	—
12	16:11:05.28	-22:22:57.3	—	20.526±0.051	19.123±0.027	18.461±0.192	17.313±0.109	20.000±	—	—
13	16:11:27.61	-22:43:33.6	—	15.913±0.003	15.085±0.002	14.469±0.005	13.867±0.005	—	—	—
14	16:12:44.88	-23:02:14.0	—	18.168±0.009	16.973±0.007	16.264±0.022	15.622±0.025	—	—	—
15	16:12:57.41	-23:05:55.4	—	19.989±0.032	18.706±0.020	18.137±0.116	17.326±0.119	—	—	—
16	16:13:30.35	-22:44:06.7	—	15.273±0.002	14.590±0.002	13.965±0.004	13.599±0.004	15.840±0.007	—	—

imposed a simultaneous detection in all four *YJHK* passbands (Lodieu et al. 2007).

The next step was to crossmatch this catalogue of new candidates with the methane imaging data from WIRCam to look at the cluster sequence with respect to the methane colour (Figure 2). We crossmatched the full deep USco survey and the methane survey with a matching radius of 2 arcsec. The total number of common sources is 65,152 over one square degree. We also crossmatched the known spectroscopic members with the full methane survey, returning only one source, USco J160918.69–222923.7 (L1; Lodieu et al. 2008) out of the 30 members covered by WIRCam (green open square in Figure 2). We identified another object with methane photometry, USco J160956.34–222245.6, classified as a field L2 dwarf by Lodieu et al. (2008). Its methane colour is bluer than the young L1 type belonging to USco. We should mention that the $\text{CH}_{4\text{off}}$ and $\text{CH}_{4\text{on}}$ images saturate at about 16 mag, corresponding to roughly 17.7 and 16.7 mag in *Y* and *J*, respectively. As a consequence, none of the bright members and new candidates will be retrieved in the methane survey. We found that five of the seven faintest ($Y \geq 20$ mag) new candidates from the *YJ* survey have methane photometry (filled red dots in Figure 2).

5 PROPER MOTIONS

In this section, we take advantage of the large epoch difference between the GCS SV and the deep *YJ* survey to estimate proper motions for cluster member candidates listed in Table 7. The baseline is of the order of three years: the GCS SV data were obtained on 12 and 19 April 2005 whereas the deep survey was carried out on 4 and 5 May 2008 taking the *J*-band observations as reference. The baseline between the deep *YJ* survey and methane observations is less than two

months, too small to infer any reliable membership based on proper motion for the T dwarf candidates in Table 5. The typical accuracy on the proper motion measurement is better than 10 mas/yr for the sources with photometric detections of 20σ or more. This centroiding accuracy decrease linearly with the signal-to-noise, implying that sources with 10σ and 5σ detections have proper motion errors of the order of 14–18 mas/yr (depending on the epoch difference; 3 or 4 years) and 30 mas/yr for objects fainter than $J = 19$ mag using the 4 year baseline, respectively. Thus, the faintest candidate identified in this survey, USco J160835.54–225311.4, and classified as a proper motion non member is consistent with the USco mean motion within the error bars (Table 8).

There are 13 *YJ* candidates with GCS SV astrometry. We computed their proper motions using the GCS SV as first epoch and the deep *YJ* survey as second epoch. The proper motions in right ascension and declination are listed in Table 8. We show that 11 out of 13 photometric candidates exhibit proper motions within 3σ of the USco mean proper motion ($-11, -25$ mas/yr), implying that they remain as probable members. We should emphasise that the same conclusion is reached when using the GCS DR8 instead of the deep *YJ* as a second epoch. One of the proper motion non members, USco J161257.41–230555.4, was classified as a photometric non member earlier in our analysis.

The one year baseline between the deep *YJ* survey and the GCS DR8 suggests that USco J160716.98–224214.1 may be a proper motion non member despite the large uncertainty. Adding this argument to its rejection as a photometric member (Section 4), this object very likely does not belong to the USco association.

Table 8. Coordinates, observing dates, and estimated proper motions in right ascension and declination for the 13 candidates common to the deep *YJ* survey, the GCS DR8, and the GCS SV databases. The last column provide additional comments based on additional data discussed in the text: the terminology is as follows: NM stands for non member; PM for proper motion; photNM for photometric non member; and L11a for Lodieu et al. (2011).

ID	R.A. (deep)	dec (deep)	Epoch deep	Epoch DR8	Epoch SV	$\mu_{\alpha \cos \delta}$	μ_{δ}	Comments
9	16:09:03.86	-22:23:22.2	2008.34153	2009.33973	2005.29863	-23.57	-39.19	PM_NM
11	16:10:00.17	-23:12:19.3	2008.34426	2008.40713	2005.29863	-6.27	+2.42	NM_L11a
16	16:13:30.35	-22:44:06.7	2008.34426	2009.33973	2005.27945	-7.91	-9.57	PM_NM
13	16:11:27.61	-22:43:33.6	2008.34426	2009.33973	2005.27945	-4.27	-8.92	
10	16:09:05.67	-22:45:16.7	2008.34153	2009.33973	2005.29863	-0.88	-4.58	PM_borderline
1	16:06:30.92	-22:58:15.2	2008.34153	2008.40713	2005.29863	+2.31	-1.81	
14	16:12:44.88	-23:02:14.0	2008.34426	2008.40713	2005.27945	-13.11	-4.20	
4	16:07:55.42	-22:33:52.5	2008.34153	2009.33973	2005.29863	-24.46	-6.83	photNM
15	16:12:57.41	-23:05:55.4	2008.34153	2008.40713	2005.27670	+92.03	+8.75	photNM
7	16:08:42.38	-22:23:25.9	2008.34153	2009.33973	2005.29863	-11.71	-24.37	photNM
5	16:08:12.99	-23:04:31.4	2008.34153	2008.40713	2005.29863	-10.50	-20.09	
12	16:11:05.28	-22:22:57.3	2008.34426	2009.33973	2005.27945	-3.69	-14.03	photNM
6	16:08:35.54	-22:53:11.4	2008.34153	2009.33973	2005.29863	+44.36	-3.29	PM_NM

6 SPECTROSCOPIC FOLLOW-UP

In this section, we analyse the optical and near-infrared cross-dispersed spectra of four candidates identified in the 0.95 square degree area in the central part of the USco association common to the *YJ* and methane surveys.

6.1 Spectral analysis

In this section, we discuss the spectral properties of the four photometric candidates whose spectral energy distribution resembles that of L-type dwarfs.

The X-Shooter spectra of USco J160755.42–223352.52 and USco J160842.38–222325.86 have much better signal-to-noise than the other two sources. In the visible arm, the spectrum of USco J160842.38–222325.86 appears redder towards longer wavelengths, suggesting a later spectral type. The same trend is seen in the *J*-band region of the near-infrared arm whereas the *H*-band region appears quite similar. The near-infrared spectra of the two fainter photometric candidates are very similar to the spectrum of USco J160755.42–223352.52 despite the low signal-to-noise and the presence of many sky lines not well removed by the current version of the X-shooter pipeline. A more quantitative comparison is unfortunately not possible at this stage.

All of the four photometric candidates discussed here look like field mid- to late-L dwarfs. For example, they do not harbour the peaked-shape in the *H*-band typical of young L-type brown dwarfs identified in star forming regions (e.g. Allers et al. 2007; Lodieu et al. 2008), pointing towards age later than a few hundred Myrs. We compared our spectra to low resolution near-infrared of “template” brown dwarfs observed with the NIRSPEC spectrograph (McLean et al. 2003). We found that the *J* and *H* regions of our near-infrared spectra are best fit by the NIRSPEC spectra of 2MASS J15074769–1627386 (L5; Reid et al. 2000; Kirkpatrick et al. 2000; Knapp et al. 2004) overplotted in red on the best signal-to-noise spectra in Fig. 4. The uncertainty on the spectral type is of the order of one subclass, suggesting that the four object are L4–L6 field dwarf. The

optical spectrum of USco J160755.42–223352.52 confirm such a spectral type whereas USco J160842.38–222325.86 may be slightly later by 1 or 2 subclass, possibly L8 according to its optical shape.

Moreover, we measured a few gravity-sensitive doublets, including the KI doublets at 1.168/1.177 and 1.243/1.254 microns and the NaI doublet at 1.268 microns, to add constraints on the age of these L-type candidates and their membership of the USco association. These doublets have been extensively used in the literature to disentangle field brown dwarfs from young substellar objects (e.g. McGovern et al. 2004; Allers et al. 2007; Cushing et al. 2005; Lodieu et al. 2008; Lafrenière et al. 2010; Bonnefoy et al. 2010). We resolved the KI doublets at the resolution of the X-Shooter spectra but not the NaI doublet which is also affected by a strong sky line which removes about 10% of the flux in this region. We measured their pseudo-equivalent widths after smoothing the *J*-band spectra by a factor of 20 with a weighted sum procedure. We used the task `SPLIT` to carry out such measurements. Typical error bars on the measurements are 1–2 Å for the two brightest sources and ~ 2 –3 Å for the faintest candidates. The values reported in Table 9 for these three doublets confirm that these sources are old L dwarfs because of the presence of strong equivalent widths. Hence, we classify these four photometric candidates as mid- to late-L field dwarfs and reject them as members of the USco association.

6.2 Properties of the quasar

In this section we discuss the properties of the quasar found in our search for ultracool brown dwarfs in USco. It is interesting to see that a methane search for substellar objects can be contaminated by quasars at low redshift (Goldman et al. 2010). Its spectrum is shown in Fig. 6

In the extracted spectrum of USco J160900.40–231150.95, we identify strong, broad Balmer emission lines typical of quasars. As shown in Fig. 6, narrower Oxygen, Neon, and Carbon lines are found in addition to the Balmer

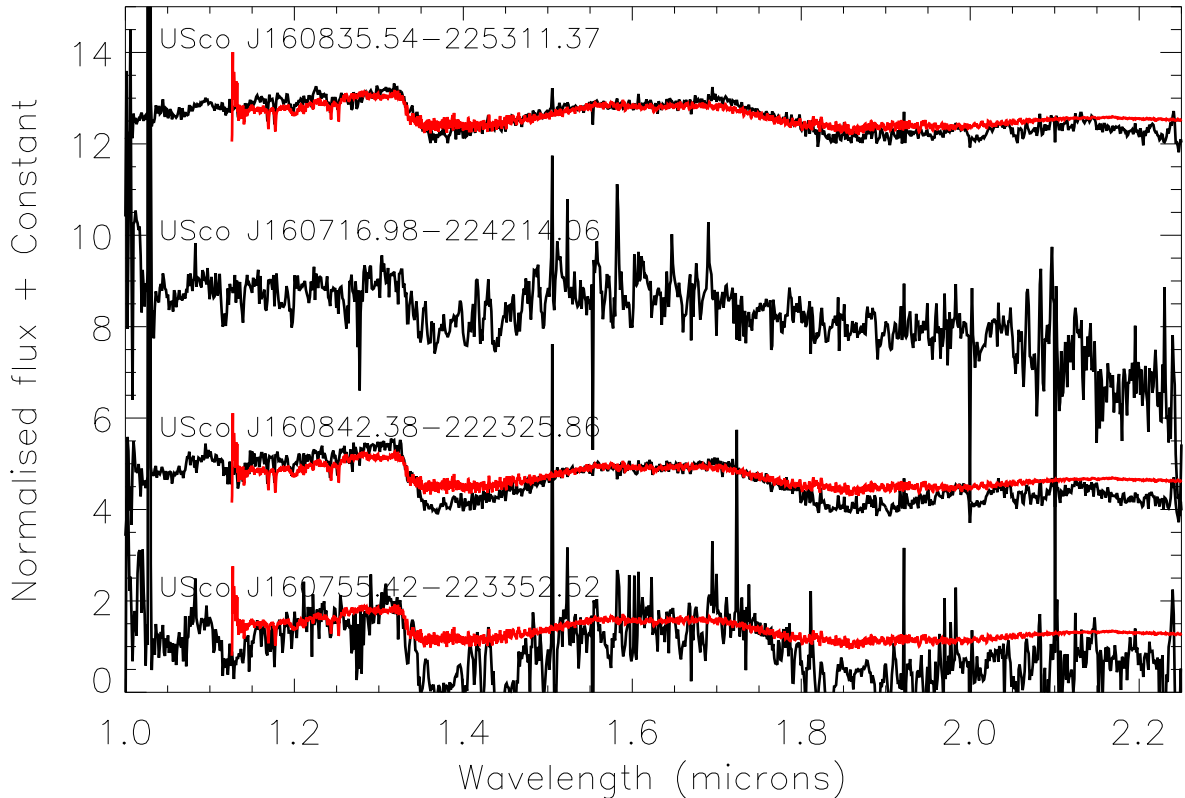


Figure 4. X-shooter spectra of four photometric candidates covering the 1.0–2.5 micron wavelength. The spectra have been normalised at 1.265 microns and smoothed by a factor of 20 with using a weighted sum procedure, resulting in an improved signal-to-noise and a resolution of ~ 250 in the near-infrared. From bottom to top, we show USco J160755.42–223352.52, USco J160842.38–222325.86, USco J160835.54–225311.37, and USco J160716.98–224214.06. Overplotted in red as a comparison is the near-infrared spectrum of the known field L5 dwarf, 2MASS J15074769–1627386.

Table 9. Pseudo-equivalent widths of gravity-sensitive doublets for four photometric candidates identified in USco. We give the equivalent widths in \AA for each component of the three doublets: KI at 1.168/1.177 and 1.243/1.254 microns and the sum of the NaI doublet at 1.268 microns.

USco J...	KI 1.168/1.177	KI 1.243/1.254	NaI 1.268
160716.98–224214.06	12.6+13.4	12.6+15.0	13.7
160755.42–223352.52	9.2+8.2	8.4+8.4	6.5
160835.54–225311.37	19.4+9.3	7.3+7.5	12.7
160842.38–222325.86	9.2+12.2	7.4+6.2	7.1

lines, and from these lines we determine an average redshift of 0.8789 ± 0.0002 .

Compared to a composite spectrum of quasars from the SDSS Vanden Berk et al. (2001) the $H\beta$ and [OIII] $\lambda\lambda 4959, 5007$ lines have similar strengths relative to the continuum flux, while the $H\alpha$ emission is stronger by a factor of ~ 8 . Apart from the strong lines, the continuum slope is consistent with the average quasar spectral slope. These characteristics arise when the emission from the quasar broad

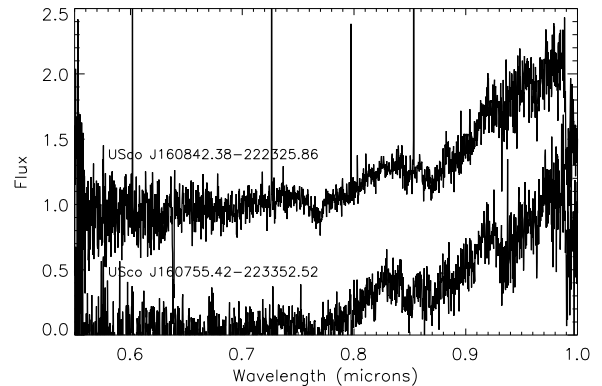


Figure 5. X-shooter spectra of two photometric candidates covering the 0.6–1.0 micron wavelength. The spectra have been normalised at 9200 \AA and smoothed by a factor of 20 with a weighted sum procedure, resulting to a resolution of ~ 200 in the optical.

line region is partly absorbed by dust in a non-uniform dust configuration, which allows the quasar continuum emission to pass through relatively unabsorbed. Since $H\alpha$ falls within

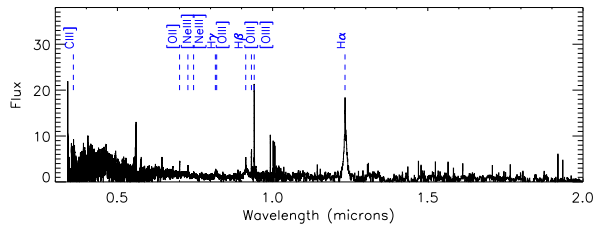


Figure 6. X-shooter optical and near-infrared spectrum of the quasar at redshift ~ 0.88 found during our photometric search for low-mass brown dwarf members in USco. The main emission lines are marked.

the J band at the redshift of the quasar, the red $Y - J$ colour is dominated by the excess emission from this line.

7 DISCUSSION: TESTING THE FRAGMENTATION LIMIT AT 5 MYR

In this section, we summarise the results and put our results into context discussing the possible turn down of the mass function in the context of theory of fragmentation limit.

Out of the 16 candidates identified in the deep YJ survey presented here, we are left with four candidates with $YJHK$ photometry and proper motions consistent with the USco mean motion. Three of these four candidates are brighter than the GCS limit and outside the GCS coverage; one being fainter and new. We identified another photometric candidates based on its $Y - J$ colour only as well as five potential young T dwarfs in the methane survey without optical counterpart.

Our new deep YJ survey is approximately 2 magnitudes deeper in both Y and J filters than the 5σ completeness limits of the UKIDSS GCS. We identified one candidate with a magnitude comparable to the depth of the GCS and another at the limit of the deep YJ survey, suggesting that this new study has revealed at most one new low-mass brown dwarf in USco. Indeed we do not confirm any new candidates in the $Y = 20$ – 22 mag range and identified only one new photometric candidate (not counting the T dwarf candidates that require additional follow-up). The lowest mass brown dwarf identified in the GCS and confirmed spectroscopically (Lodieu et al. 2008) has an effective temperature of ~ 1800 K and a mass of $\sim 8 M_{\text{Jup}}$ according to the DUSTY models (Chabrier et al. 2000). If we consider that our new survey is roughly two magnitudes deeper, this would correspond to masses of 3–4 M_{Jup} following predictions from the dust-free COND models (Baraffe et al. 2002). Overall, this result is puzzling because we find many candidates that look like USco photometric members in various colour-magnitude diagrams which we rejected later on the basis of their astrometry and/or spectroscopy.

In our studies of the central region of the USco association, we confirmed spectroscopically 14 members with masses in the 0.02 – $0.01 M_{\odot}$ over 6.5 square degrees (Lodieu et al. 2007, 2008, 2011). This mass range corresponds roughly to $J = 15$ – 17.2 mag according to the DUSTY models of the Lyon group (Chabrier et al. 2000). We want to address the following question: how many new brown dwarfs

do we expect down to the limit of our deep YJ survey covering 1.7 square degree. If we assume a constant mass function in the next mass bin chosen as 0.01 – $0.005 M_{\odot}$ (corresponding to $J \sim 17.2$ – 21.5 mag), we would expect $14/6.5 \times 1.7 = 3.7$ members. However, if we extrapolate the field mass function in the same mass bin considering that we found a factor of three difference in the number of objects compared to our spectroscopic mass function (Lodieu et al. 2011), we would expect 1.2 objects in our deep survey. Hence, the one photometric candidate we extracted in our deep survey is consistent with the low limit of those predictions.

We estimated the number of field T0–T8 dwarfs expected in our deep YJ survey covering 1.7 square degrees down to $J = 21.5$ mag. Pinfield et al. (2008) found 26–44 T0–T8 dwarfs in 280 square degrees surveyed by the UKIDSS Large Area Survey down to $J = 19$ mag. Scaling these numbers to the area covered by our YJ survey and the depth, we estimate that our survey may be contaminated by 5.0–6.6 to 8.4–11.1 field T dwarfs. However, if we consider only the methane coverage which is designed to focus on T dwarfs and which is shallower than the deep YJ survey ($H \sim 20.2$ – 20.3 mag), we would expect 1–2 T dwarfs compared to our five candidates listed in Table 5. These numbers suggest a high level of contamination of at least 20 to 40% among our T dwarf candidates. This result is in line with the classification of four of the faint photometric candidates as spectroscopic non members.

Although we are missing additional membership constraints on the potential T dwarf candidates presented here, we are in a position to discuss a possible turn down in the mass function as we approach the fragmentation limit in USco as our deep survey has not revealed any new spectroscopic late-L or T dwarf. Independent works in σ Orionis by Bihain et al. (2009) and Peña Ramírez et al. (2011) presented deep infrared and methane surveys with similar depths in terms of mass as our study where the numbers of T-type member candidates seem to fall down below ~ 6 Jupiter masses because none of the T dwarfs announced to date in this region has been unambiguously confirmed astrometrically and spectroscopically. However, the spectral sequence in σ Orionis extends down to late-L dwarfs (Barrado y Navascués et al. 2001; Martín et al. 2001) while our USco sequence currently stops at early-L dwarfs or possibly mid-L if we include the planetary-mass companion found by Lafrenière et al. (2010) around a solar analog despite the possible excess of brown dwarfs seen in USco (Preibisch & Zinnecker 2002; Slesnick et al. 2008; Lodieu et al. 2011). Our survey seems to favour a turn down in the USco mass function below 10 Jupiter masses but a wider survey as deep the one presented here is needed to improve the statistics and confirm this possible turn down. We cannot yet argue that we have reached the fragmentation limit in USco. To conclude, T-type members with masses below a few Jupiter masses seem to be rare at very young ages (< 10 Myr), placing an upper limit on the smallest fragments that star formation processes can form (Low & Lynden-Bell 1976; Rees 1976; Boss 2001).

8 SUMMARY AND OUTLOOK

We have presented the outcome of deep photometric survey of 0.95 square degree in the USco association combining near-infrared and methane imaging. We identified 16 new candidates in 1.7 square degrees surveyed in Y and J , leaving four probable members including at the limit of our survey after applying additional photometric and astrometric constraints from various surveys taken at different epochs. Near-infrared spectroscopy of four of the faintest candidates has shown that their are old field mid-L dwarfs contaminating our photometric search while the other is a quasar at low redshift. Moreover, we also extracted five potential methane T dwarf candidates without optical counterparts and reasonable $Y - J$ colours. The lack of new spectroscopic members in USco in a survey two magnitudes deeper than the UKIDSS GCS points towards a turn down in the USco mass function or may suggest that we have reached the fragmentation limit in the association.

Spectroscopy of these faint T dwarf candidates is difficult with ground-based facility, suggesting that these sources may be ideal targets for the James Webb Space Telescope and the future E-ELT. Proper motion confirmation is a more affordable option to confirm the membership of these T dwarfs to the USco association very soon with a second epoch. Furthermore, the advent of the Visible Infrared Survey Telescope for Astronomy (VISTA; Emerson 2001) will allow to cover larger areas in smaller numbers of pointing to improve the statistics and confirm (or otherwise) that we have reached the fragmentation limit in USco.

ACKNOWLEDGMENTS

NL was funded by the Ramón y Cajal fellowship number 08-303-01-02 and the national program AYA2010-19136 funded by the Spanish ministry of science and innovation. NL thanks Loïc Albert and Patrick Hudelot for their help in the preparation of the observing blocks and the data reduction, respectively. LS thanks NL for funding her one week stay at the IAC, Tenerife.

This work made use of data taken with various telescopes and instruments in visitor and service mode. The Y, J infrared data with Wide Field Camera (WFCAM) on the United Kingdom Infrared Telescope (UKIRT), operated by the Joint Astronomy Centre (JAC) on behalf of the Science and Technology Facilities Council (STFC) of the United Kingdom (UK). The methane ON and OFF data are based on observations obtained with WIRCAM, a joint project of CFHT, Taiwan, Korea, Canada, France, and the Canada France Hawaii Telescope (CFHT) which is operated by the National Research Council (NRC) of Canada, the Institute National des Sciences de l'Univers of the Centre National de la Recherche Scientifique of France, and the University of Hawaii. We acknowledge the Terapix team at the Institut d'Astrophysique de Paris that produced the images and catalogues used in this work, with special thanks to Patrick Hudelot. The X-Shooter spectroscopy is based on observations made with ESO telescopes at the La Silla Paranal Observatory under programme ID 385.C-0950 in service mode.

This research has made use of the Simbad and Vizier databases, operated at the Centre de Données As-

tronomiques de Strasbourg (CDS), and of NASA's Astrophysics Data System Bibliographic Services (ADS).

This publication makes use of data products from the Two Micron All Sky Survey (2MASS), which is a joint project of the University of Massachusetts and the Infrared Processing and Analysis Center/California Institute of Technology, funded by the National Aeronautics and Space Administration and the National Science Foundation.

This publication makes use of data products from the Wide-field Infrared Survey Explorer, which is a joint project of the University of California, Los Angeles, and the Jet Propulsion Laboratory/California Institute of Technology, funded by the National Aeronautics and Space Administration.

REFERENCES

- Allers K. N., et al. 2007, *ApJ*, 657, 511
 Alves de Oliveira C., Moraux E., Bouvier J., Bouy H., Marmo C., Albert L., 2010, *A&A*, 515, A75
 Ardila D., Martín E., Basri G., 2000, *AJ*, 120, 479
 Baraffe I., Chabrier G., Allard F., Hauschildt P. H., 1998, *A&A*, 337, 403
 Baraffe I., Chabrier G., Allard F., Hauschildt P. H., 2002, *A&A*, 382, 563
 Barrado y Navascués D., Zapatero Osorio M. R., Béjar V. J. S., Rebolo R., Martín E. L., Mundt R., Bailer-Jones C. A. L., 2001, *A&A*, 377, L9
 Bertin E., Arnouts S., 1996, *A&AS*, 117, 393
 Bihain G., Rebolo R., Zapatero Osorio M. R., Béjar V. J. S., Caballero J. A., 2010, *A&A*, 519, A93
 Bihain G., et al. 2009, *A&A*, 506, 1169
 Bonnefoy M., Chauvin G., Rojo P., Allard F., Lagrange A.-M., Homeier D., Dumas C., Beuzit J.-L., 2010, *A&A*, 512, A52
 Boss A. P., 2001, *ApJL*, 551, L167
 Burgasser A. J., Kirkpatrick J. D., McGovern M. R., McLean I. S., Prato L., Reid I. N., 2004, *ApJ*, 604, 827
 Burgess A. S. M., Moraux E., Bouvier J., Marmo C., Albert L., Bouy H., 2009, *A&A*, 508, 823
 Burrows A., Marley M., Hubbard W. B., Lunine J. I., Guillot T., Saumon D., Freedman R., Sudarsky D., Sharp C., 1997, *ApJ*, 491, 856
 Casali M., et al. 2007, *A&A*, 467, 777
 Casewell S. L., Dobbie P. D., Hodgkin S. T., Moraux E., Jameson R. F., Hambly N. C., Irwin J., Lodieu N., 2007, *MNRAS*, 378, 1131
 Chabrier G., 2003, *PASP*, 115, 763
 Chabrier G., Baraffe I., 1997, *A&A*, 327, 1039
 Chabrier G., Baraffe I., Allard F., Hauschildt P., 2000, *ApJ*, 542, 464
 Collins R., Cross N. J., Sutorius E., Read M., Hambly N. C., 2009, in D. A. Bohlender, D. Durand, & P. Dowler ed., *Astronomical Society of the Pacific Conference Series* Vol. 411 of *Astronomical Society of the Pacific Conference Series*, Automated Data Releases for the WFCAM Science Archive. p. 226
 Cross N. J. G., Collins R. S., Hambly N. C., Blake R. P., Read M. A., Sutorius E. T. W., Mann R. G., Williams P. M., 2009, *MNRAS*, 399, 1730

- Cushing M. C., Rayner J. T., Vacca W. D., 2005, *ApJ*, 623, 1115
- Cutri R. M., et al. 2003, 2MASS All Sky Catalog of point sources, 2246
- de Bruijne J. H. J., Hoogerwerf R., Brown A. G. A., Aguilar L. A., de Zeeuw P. T., 1997, in *ESA SP-402: Hipparcos - Venice '97 Improved Methods for Identifying Moving Groups*. pp 575–578
- de Zeeuw P. T., Hoogerwerf R., de Bruijne J. H. J., Brown A. G. A., Blaauw A., 1999, *AJ*, 117, 354
- Dobbie P. D., Kenyon F., Jameson R. F., Hodgkin S. T., Pinfield D. J., Osborne S. L., 2002, *MNRAS*, 335, 687
- Dobbie P. D., Pinfield D. J., Jameson R. F., Hodgkin S. T., 2002, *MNRAS*, 335, L79
- D’Odorico S., et al. 2006, in *Society of Photo-Optical Instrumentation Engineers (SPIE) Conference Series Vol. 6269 of Society of Photo-Optical Instrumentation Engineers (SPIE) Conference Series, X-shooter UV- to K-band intermediate-resolution high-efficiency spectrograph for the VLT: status report at the final design review*
- Emerson J. P., 2001, in R. Clowes, A. Adamson, & G. Bromage ed., *The New Era of Wide Field Astronomy Vol. 232 of Astronomical Society of the Pacific Conference Series, VISTA - Project Status of the Visible and Infrared Survey Telescope for Astronomy*. p. 339
- Geers V., Scholz A., Jayawardhana R., Lee E., Lafrenière D., Tamura M., 2011, *ApJ*, 726, 23
- Goldman B., Marsat S., Henning T., Clemens C., Greiner J., 2010, *MNRAS*, 405, 1140
- Goldoni P., Royer F., François P., Horrobin M., Blanc G., Vernet J., Modigliani A., Larsen J., 2006, in *Society of Photo-Optical Instrumentation Engineers (SPIE) Conference Series Vol. 6269 of Presented at the Society of Photo-Optical Instrumentation Engineers (SPIE) Conference, Data reduction software of the X-shooter spectrograph*
- Hambly N. C., et al. 2008, *MNRAS*, 384, 637
- Hewett P. C., Warren S. J., Leggett S. K., Hodgkin S. T., 2006, *MNRAS*, 367, 454
- Irwin M., Lewis J., 2001, *New Astronomy Review*, 45, 105
- Irwin M. J., et al. 2004, eds, *Optimizing Scientific Return for Astronomy through Information Technologies*. Edited by Quinn, Peter J.; Bridger, Alan. *Proceedings of the SPIE, Volume 5493*, pp. 411-422 (2004). *VISTA data flow system: pipeline processing for WFCAM and VISTA*. pp 411–422
- Kirkpatrick J. D., et al. 2000, *AJ*, 120, 447
- Knapp G. R., Leggett S. K., Fan X., Marley M. S., Geballe T. R., Golimowski D. A., Finkbeiner D., Gunn J. E., 21 co-authors 2004, *AJ*, 127, 3553
- Kunkel M., 1999, Ph.D. Thesis, Julius-Maximilians-Universität Würzburg
- Lafrenière D., Jayawardhana R., van Kerkwijk M. H., 2010, *ApJ*, 719, 497
- Lawrence A., et al. 2007, *MNRAS*, 379, 1599
- Leggett S. K., et al. 2010, *ApJ*, 710, 1627
- Liu M. C., Leggett S. K., Chiu K., 2007, *ApJ*, 660, 1507
- Lodieu N., Dobbie P. D., Deacon N. R., Hodgkin S. T., Hambly N. C., Jameson R. F., 2007, *MNRAS*, 380, 712
- Lodieu N., Dobbie P. D., Hambly N. C., 2011, *A&A*, 527, A24
- Lodieu N., Hambly N. C., Jameson R. F., 2006, *MNRAS*, 373, 95
- Lodieu N., Hambly N. C., Jameson R. F., Hodgkin S. T., 2008, *MNRAS*, 383, 1385
- Lodieu N., Hambly N. C., Jameson R. F., Hodgkin S. T., Carraro G., Kendall T. R., 2007, *MNRAS*, 374, 372
- Low C., Lynden-Bell D., 1976, *MNRAS*, 176, 367
- Luhman K. L., Hernández J., Downes J. J., Hartmann L., Briceño C., 2008, *ApJ*, 688, 362
- Mainzer A., et al. 2011, *ApJ*, 726, 30
- Marocco F., et al. 2010, *A&A*, 524, A38
- Marsh K. A., Plavchan P., Kirkpatrick J. D., Lowrance P. J., Cutri R. M., Velusamy T., 2010, *ApJ*, 719, 550
- Martín E. L., Delfosse X., Guieu S., 2004, *AJ*, 127, 449
- Martin E. L., et al. 2010, *A&A*, 517, A53
- Martín E. L., Zapatero Osorio M. R., Barrado y Navascués D., Béjar V. J. S., Rebolo R., 2001, *ApJL*, 558, L117
- McGovern M. R., Kirkpatrick J. D., McLean I. S., Burgasser A. J., Prato L., Lowrance P. J., 2004, *ApJ*, 600, 1020
- McLean I. S., McGovern M. R., Burgasser A. J., Kirkpatrick J. D., Prato L., Kim S. S., 2003, *ApJ*, 596, 561
- Modigliani A., et al. 2010, in *Society of Photo-Optical Instrumentation Engineers (SPIE) Conference Series Vol. 7737 of Presented at the Society of Photo-Optical Instrumentation Engineers (SPIE) Conference, The X-shooter pipeline*
- Monet D. G., et al. 2003, *AJ*, 125, 984
- Moraux E., Bouvier J., Stauffer J. R., Cuillandre J.-C., 2003, *A&A*, 400, 891
- Patten B. M., et al. 2006, *ApJ*, 651, 502
- Peña Ramírez K., Zapatero Osorio M. R., Béjar V. J. S., Rebolo R., Bihain G., 2011, *ArXiv e-prints*
- Pinfield D. J., Burningham B., Tamura M., Leggett S. K., Lodieu N., Lucas P. W., Mortlock D. J., 28 co-authors 2008, *MNRAS*, 390, 304
- Preibisch T., Guenther E., Zinnecker H., 2001, *AJ*, 121, 1040
- Preibisch T., Guenther E., Zinnecker H., Sterzik M., Frink S., Roeser S., 1998, *A&A*, 333, 619
- Preibisch T., Zinnecker H., 2002, *AJ*, 123, 1613
- Puget P., et al. 2004, in A. F. M. Moorwood & M. Iye ed., *Society of Photo-Optical Instrumentation Engineers (SPIE) Conference Series Vol. 5492 of Society of Photo-Optical Instrumentation Engineers (SPIE) Conference Series, WIRCAM: the infrared wide-field camera for the Canada-France-Hawaii Telescope*. pp 978–987
- Rees M. J., 1976, *MNRAS*, 176, 483
- Reid I. N., Kirkpatrick J. D., Gizis J. E., Dahn C. C., Monet D. G., Williams R. J., Liebert J., Burgasser A. J., 2000, *AJ*, 119, 369
- Scholz A., Geers V., Jayawardhana R., Fissel L., Lee E., Lafreniere D., Tamura M., 2009, *ApJ*, 702, 805
- Scholz A., Jayawardhana R., 2008, *ApJL*, 672, L49
- Skrutskie M. F., et al. 2006, *AJ*, 131, 1163
- Slesnick C. L., Carpenter J. M., Hillenbrand L. A., 2006, *AJ*, 131, 3016
- Slesnick C. L., Hillenbrand L. A., Carpenter J. M., 2008, *ApJ*, 688, 377
- Tinney C. G., Burgasser A. J., Kirkpatrick J. D., McElwain M. W., 2005, *AJ*, 130, 2326
- Tokunaga A. T., Simons D. A., Vacca W. D., 2002, *PASP*, 114, 180

- Vanden Berk D. E., et al. 2001, AJ, 122, 549
Vrba F. J., et al. 2004, AJ, 127, 2948
Walter F. M., Vrba F. J., Mathieu R. D., Brown A., Myers
P. C., 1994, AJ, 107, 692
Wright E. L., et al. 2010, AJ, 140, 1868
Zapatero Osorio M. R., Béjar V. J. S., Martín E. L., Re-
bolo R., Barrado y Navascués D., Mundt R., Eislöffel J.,
Caballero J. A., 2002, ApJ, 578, 536
Zapatero Osorio M. R., Béjar V. J. S., Bihain G., 10 co-
authors 2008, A&A, 477, 895

This paper has been typeset from a $\text{\TeX}/\text{\LaTeX}$ file prepared
by the author.